COMPUTATIONAL CONVECTION THERMAL ANALYSIS ON SPINNING MICROFLUIDIC DISK DIGITAL POLYMERASE CHAIN REACTION PLATFORM

by

Cristian Esteban Clavijo

A thesis submitted to the faculty of
The University of Utah
in partial fulfilment of the requirements for the degree of

Master of Science

Department of Mechanical Engineering

The University of Utah

December 2012

The University of Utah Graduate School

STATEMENT OF THESIS APPROVAL

The thesis of **Cristian Esteban Clavijo**

has been approved by the following supervisory committee members:

Timothy Ameel	, Chair	**10/18/12** Date Approved
Bruce Gale	, Member	**10/18/12** Date Approved
Peter Alfeld	, Member	**10/18/12** Date Approved

and by **Timothy Ameel**, Chair of

the Department of **Mechanical Engineering**

and by Charles A. Wight, Dean of The Graduate School.

ABSTRACT

There have been tremendous advancements in the field of genetic engineering within the past century. Digital Polymerase Chain Reaction (PCR) is a molecular diagnostic process, extensively used in genetics research, in which a single DNA sequence per control volume is amplified by undergoing thermal cycling between two temperatures limits, generally 55 °C and 95 °C. This paper presents an analysis of the convection thermal effects associated with different design parameters for a spinning digital PCR disk containing a helix micro-channel containing a thousand nano-wells, which serve as the control volumes for the DNA solution. Further understanding and management of these design parameters is needed to optimize the design and operation of the digital PCR technology. The parameters studied in this work are the location, Reynolds number and temperature of the heating/cooling air source, the PCR disk spinning rate, and the thermocycler volume size. Changes in these parameters significantly affect the heating and cooling cycle rates, as well as the temperature uniformity of the disk. The impingement location of the air jet on the disk has a significant impact on the heating process time (9% maximum change). However, the impingement location dramatically affects temperature uniformity on the disk (173% maximum change). The impinging air jet Reynolds number contributed to both process time and temperature uniformity by a 90% change. Temperature uniformity was adversely affected for Reynolds numbers greater than $30x10^3$.

To Frank, Julia and Vanessa

TABLE OF CONTENTS

LIST OF FIGURES

ACKNOWLEDGEMENTS

First, I want to thank my parents, Frank Clavijo and Julia Angeles, for their perpetual support and motivation in my academic pursuits. My little sister, Vanessa Clavijo, has been another key factor in the successful completion of this scientific endeavor, as well as other interests throughout my life. Furthermore, my family members who still reside in Peru have periodically provided priceless jolts of motivation and hope in my advancements as a leader in engineering and science outside of our home country.

In addition, I want to thank Dr. Tim Ameel for his guidance, mentoring, research efforts, and freedom he gave me to direct this project. His knowledge and experience proved to be invaluable assets in the completion of this thesis and all the work therein. I also want to thank Dr. Bruce Gale and Dr. Peter Alfeld, members of my supervisory committee, for their suggestions and recommendations throughout this project. Their unique expertise helped diversify this project and unite three different departments, namely Mechanical Engineering, Biomedical Engineering and Mathematics.

Lastly, I thank my classmates and lab mates for their input throughout the project, as well as their humor, which at times was essential to wade through such great a cause, so to speak.

CHAPTER 1

INTRODUCTION

1.1 Background

1.1.1 MEMS

Diverse and perplexing natural phenomena have always driven humans—certainly those who carry a keen penchant in furthering scientific knowledge—to explore unimaginable territories. Though for thousands of years have the celestial bodies and laws of the seemingly unending universe been studied and scrutinized, only in the last century has its contrasting, yet complementary, counterpart been explored—nanotechnology. Indeed, the nano-world and its governing laws, which differ in emphasis from macro- and even micro-level physics, are only beginning to be discovered and understood—generously speaking.

Too seldom, there comes along an inspired individual, even a science-thirsty mind, who will devote his/her life to seek insights to unanswered questions. One such great individual was Richard Feynman, a theoretical physicist well versed in the natural sciences, who in 1959 posed the question, "What would happen if we could arrange the atoms one by one the way we want them?" [1]. This critical question, its unimaginable far-reaching consequences,

and all moral and physical implications that pertain to it, continues to compel scientists and engineers today.

One direct offspring of such a loaded statement is the world of Micro-ElectroMechanical Systems (MEMS). Not to be confused with Nano-ElectroMechanical Systems (NEMS), MEMS have proven to be a step in the right direction. MEMS consist of structures ranging in size from one micrometer to several millimeters. These micro-systems are made up of micro-actuators, micro-processors and micro-sensors, and carry out processes that present several advantages over traditional engineering, such as large surface area-to-volume ratio, small control volumes, fast heat and mass transport processes, high heat transfer rates, detailed control, and environment-friendly manufacturing. Also, with inexpensive materials generally revolving around silicon-based polymers, MEMS are an attractive and versatile technology of great utility and application. MEMS have already impacted the areas of medicine, biology, chemistry and robotics, and will continue to impact other areas such as the automobile industry, the printing industry and even sustainable energy systems, to name a few.

1.1.2 Polymerase Chain Reaction

The discovery of deoxyribonucleic acid (DNA) is one of the most important and influential discoveries in human history. DNA is a double-helix structure, which generally resides in cells' nuclei, and is the physio-architectural blue print of how life forms on this planet. The ability to pry into the microscopic genetic world has opened up unlimited and unexpected horizons in diverse sciences

including medicine and molecular biology, and has even affected the distant sciences of philosophy and sociology.

As the role of DNA became clearer, and microscopic technology advanced in parallel, genetic engineering emerged—though not referred to as such until later years. One process of interest, especially in areas such as forensic science, is the amplification of DNA for easier detection and/or observation. One of the first nucleic acid amplification techniques involved the use of bacteria and took weeks to yield the sought-after results. In 1985, Nobel Prize winner Kary Mullis [3] invented a revolutionary amplifying technique, which is named Polymerase Chain Reaction (PCR). This technique has transformed and simplified the approach most molecular biology labs perform experiments involving nucleic acid quantification. In its most basic definition, PCR is an *in-vitro*, thermal-dependent DNA sequence amplifying procedure. First, a buffer solution containing the DNA template (which includes the DNA target sequence to be amplified), oligonucleotide primers, deoxynucleoside triphosphates (dNTPs) and DNA polymerase is mixed together in a small test tube [4]. The solution is first heated up to ~95°C where the double-stranded DNA is melted and separated into two single-stranded DNA templates (see Figure 1.1). This step is called denaturation. Higher temperatures can cause damage to the DNA and invalidate results. Second, the solution is lowered to ~55°C for the annealing process. At this temperature, the complementary primers attach to both ends of the target DNA sequence and initiate the DNA synthesis. Last, the primers are extended to complete the desired DNA sequence by the DNA polymerase

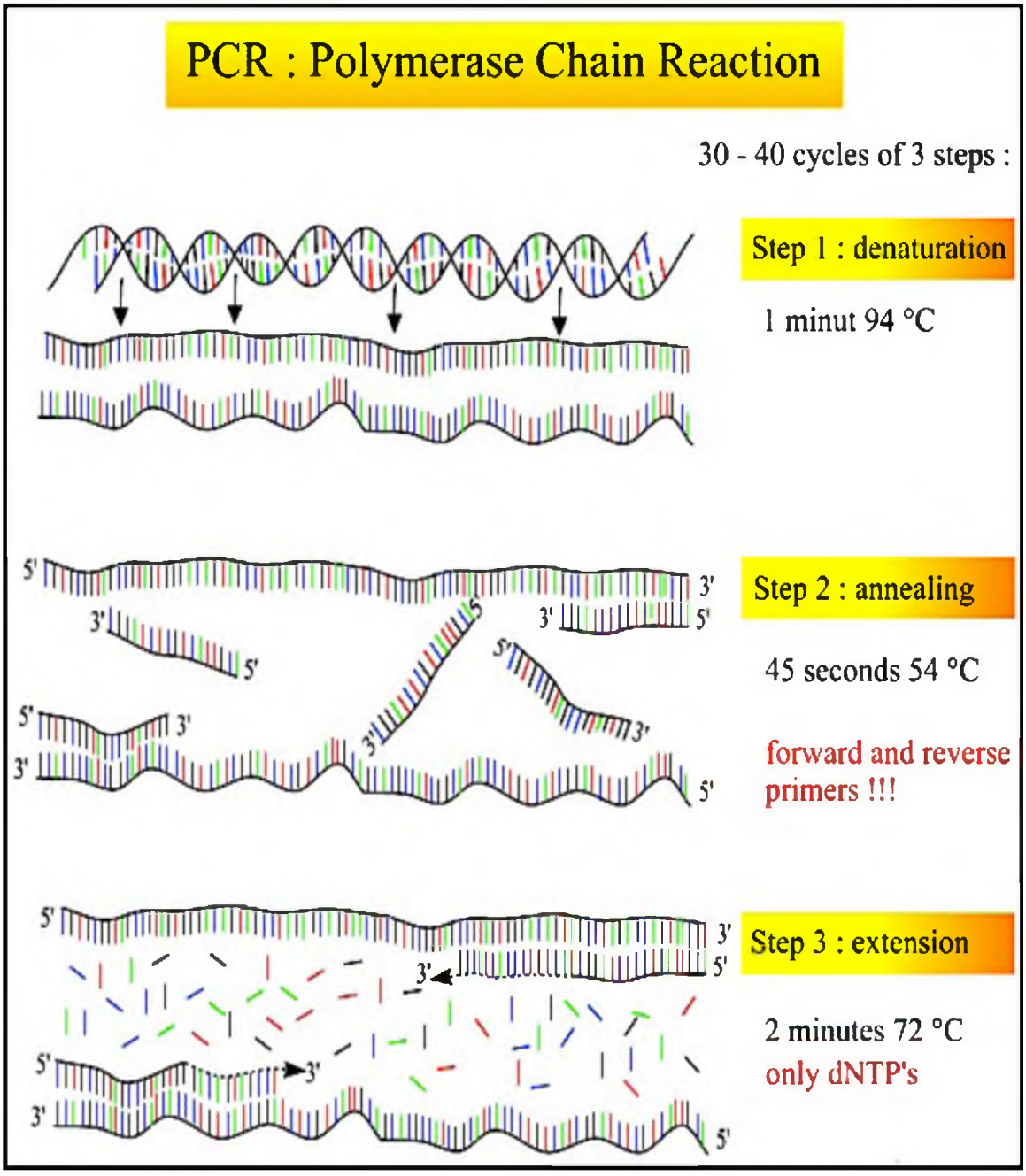

Figure 1.1: PCR sample process. The 3 steps involved in the DNA amplification process are shown for only the first cycle and only one DNA template [2].

enzyme. Taq Polymerase (having been derived from the *Thermus Aquaticus* Bacterium) is the most common enzyme used in PCR because it is thermally stable at high temperatures. This last extension step occurs at ~72°C. Each cycle increases the previous number of DNA templates exponentially. Theoretically, at the end of only 30 cycles, one single DNA template can yield over 1 billion copies as given by the formula[2] $(2^n - 2n)x$, where n is the number of cycles and x is the number of copies of the original template. Figure 1.2 provides a visual of a real-life PCR laboratory setup.

Figure 1.2: Common PCR laboratory setup. The PCR liquid solution is allocated in the clear plastic vials, which are then placed inside the thermocycler [5].
expression analysis, diagnosis of hereditary diseases, forensic science, detection

In 1999, a novel process called digital PCR was designed by Vogelstein (Vogelstein and Kinzler 1999). Digital PCR is a technique in which only one DNA template is placed into a control volume. Because digital PCR isolates single DNA templates per reaction volume, as opposed to conventional PCR, it yields more precise and reliable results. PCR technology is now used in gene of infectious disease and other areas.

1.2 Literature Review

In 2010, Sundberg et al. presented a novel microfluidic digital PCR technique [6]. This technique utilizes an inexpensive disk (~375 μm thick) made up of three thin layers. The middle layer contains a micro-channel (250 μm wide), which spirals radially outward from a central loading region. 1000 nanoliter-sized wells (33 nL) are located along this channel. The DNA solution (containing all necessary substances for the PCR process) is pipetted into the central loading region. The disc is then spun at a high rotational speed to promote outward fluid movement along the spiral channel due to centrifugation. As the solution fills the channel, it is also trapped in the wells. The solution in each well typically contains a single DNA template. Once the wells are filled, the end of the channel is thermally sealed to maintain the fluid volumes in their respective wells. A modified thermocycler heats and cools the disk by forced convection from a fan-driven air source normal to the disk. Using this technology, Sundberg et al. were able to obtain PCR cycle times of 33 seconds with 94% efficiency. Moreover, due to the simplicity of their design, they greatly

reduced cost and complexity by avoiding the use of micro-valves, pumps and extensive pipetting.

1.3 Motivation and Objective

PCR is a monumental biological advancement, but it still has many limitations. One of these drawbacks is that the concentration of the primers relative to the number of DNA templates decreases as the PCR cycles increase, thereby reducing the efficiency of the process. Another disadvantage is the degradation of the polymerase enzymes as a function of time due to thermal gradients and stress. Another limitation may be attributed to the thermal inefficacy of the heating/cooling cycling method. Clearly, a thorough understanding of the thermal behavior of the Sundberg et al. [6] microfluidic PCR system is as important as the biochemical manipulations if this technology is to reach maturity.

Sundberg's design has proven to be a novel and promising approach to digital PCR due to its low cost, fast processing time, and simplicity. However, their reported studies to date have not adequately addressed the thermal control of the system. Given the dependence of the PCR process precision, efficiency, and validity on the system thermal behavior, it is necessary to further analyze and understand the physics of the different heating/cooling mechanisms that control the process. The work reported herein presents a computational study of the spinning microfluidic digital PCR disk that is convectively heated and cooled by an orthogonal air jet. The process parameters of interest include: disc rotational speed, air jet Reynolds number, diameter, temperature, and impact

location relative to the disc center, ambient temperature, disc material properties, and PCR cycler volume (total system size). The effect of these parameters on heating/cooling times and temperature uniformity of the disc is studied. It is desirable that cycle times are low so that the total amplification process time is as short as possible. At the conclusion of a heating or cooling process, it is also desirable that the disc is uniform in temperature so that each individual fluid volume in the wells has completed the desired progression (denaturation or annealing).

1.4 References

[1] R. Feynman, *Engineering and Science*, 1959, 22 – 36.

[2] http://users.ugent.be/~avierstr/principles/pcr.html

[3] R. K. Saiki, S. Scharf, F. Faloona, K. B. Mullis, G. T. Horn, H. A. Erlich and N. Arnheim, *Science*, 1985, **230**, 1350.

[4] C. R. Newton and A. Graham, ed., in *PCR – Polymerase Chain Reaction*, Marksbury, Oxford, UK, 1994, 67.

[5] http://en.wikipedia.org/wiki/File:PCR_masina_kasutamine.jpg

[6] S. O. Sundberg, C. T. Wittwer, C. Gao and B. K. Gale, *Anal. Chem.*, 2010, **82**, 1546 – 1550.

CHAPTER 2

COMPUTATIONAL CONVECTION THERMAL ANALYSIS

2.1 Abstract

Digital Polymerase Chain Reaction (PCR) is a molecular diagnostic process in which a single DNA sequence per control volume is amplified by undergoing thermal cycling between two temperatures limits. This paper presents an analysis of the convection thermal effects associated with different design parameters for a spinning digital PCR disk containing a helix micro-channel containing a thousand nano-wells, which serve as the control volumes for the DNA solution. Proper understanding and management of these design parameters is needed to optimize the design and operation of the digital PCR technology. The parameters studied in this work are the location, Reynolds number and temperature of the heating/cooling air source, the PCR disk spinning rate, and the thermocycler volume size. Changes in these parameters significantly affect the heating and cooling cycle rates, as well as the temperature uniformity of the disk, which is a desired characteristic of the process. The impingement location of the air jet on the disk has a significant impact on the heating process time (9% maximum change). However, the impingement location dramatically affects temperature uniformity on the disk (173% maximum change), disclosing locations that yield desirable results. The impinging air jet

Reynolds number contributed an equal relative change to both heating process time and temperature uniformity (90% maximum change). Temperature uniformity was adversely affected for Reynolds numbers greater than $30x10^3$.

2.2 Introduction

2.2.1 Nucleic Acid Analysis

Advances in molecular biology have created new applications in diverse areas of nucleic acid analysis techniques, such as molecular diagnosis of disease and assessment of therapy, environmental testing, food technology, agriculture, and forensic science [1]. Other types of testing in oncologic, genetic, pharmacogenomic and other areas are quickly on the rise. Microfluidic engineering is a relatively new field that continues to find collaboration with nucleic acid analysis techniques because of its many attractive advantages such as low fluid volumes, faster analysis, precise control, and lower power consumption [2]. Polymerase Chain Reaction (PCR) is a molecular biological process whose technological development is dependent upon these two merging fields.

In PCR, a specific DNA segment is amplified creating thousands or millions of copies of itself. This process is dependent on a "hot" temperature (> 90 °C) to denature or melt the DNA double helix segments, a "cold" temperature (50 - 65 °C) where the DNA single segments assemble together with primers, and a midrange-temperature (approx. 72 °C) to optimize enzymatic activity. Digital PCR, a unique and powerful subbranch of PCR, is a highly sensitive DNA and RNA quantification technique where DNA segments are placed in individual

reaction volumes. This technique provides greater precision over quantitative real-time PCR [3]. Recently, digital PCR has been miniaturized to nano-liter volumes using microfluidics to limit the amount of DNA template in a PCR [4]. This has benefited digital PCR by reducing test costs dramatically, increasing power and sensitivity, and simplifying testing. Applications of digital PCR include identification of rare mutations within an excess of normal DNA, viral load, non-invasive prenatal testing, and aiding in next generation sequencing [2].

2.2.2 Thermal Analysis

Due to the thermal-dependent nature of the PCR process, thermal time and spatial temperature control are crucial to obtain accurate and valid results. Moreover, as stated above, the precision offered by microfluidics relies upon accurate understanding of the microphysical behavior of the system. Furthermore, having a specific mathematical model, in which the engineer or scientist can easily study the effects of different thermal and fluid parameters upon the PCR array, can provide significant design insight with no manufacturing time or expense.

2.2.3 Spinning Disk Platform

Many digital PCR processes make use of different types of droplet technologies like Fluidigm's Digital Array chips, which are composed of integrated fluidic circuits (IFC's) [5]. Digital Array IFC's use nano-scale valves and channels to position PCR solution and other relevant agents in the solution into different chambers. Pneumatic pressure is the driving force to

transport PCR solution into the respective channels [2]. Different MEMS technologies incorporate various types of valves, such as comb valves, and micro-droplets [6, 7] to isolate DNA templates in nano-liter-sized reaction chambers. A variety of digital PCR methods exist but generally they are complex and expensive. Sundberg et al. presented a novel digital PCR approach that significantly reduces chip disposable cost, microfluidic loading time, process time and instrument complexity using a spinning disk platform. The disks were approximately 4 – 6 cm in radius and 250 - 350 μm thick, as shown in Figure 2.1.A.

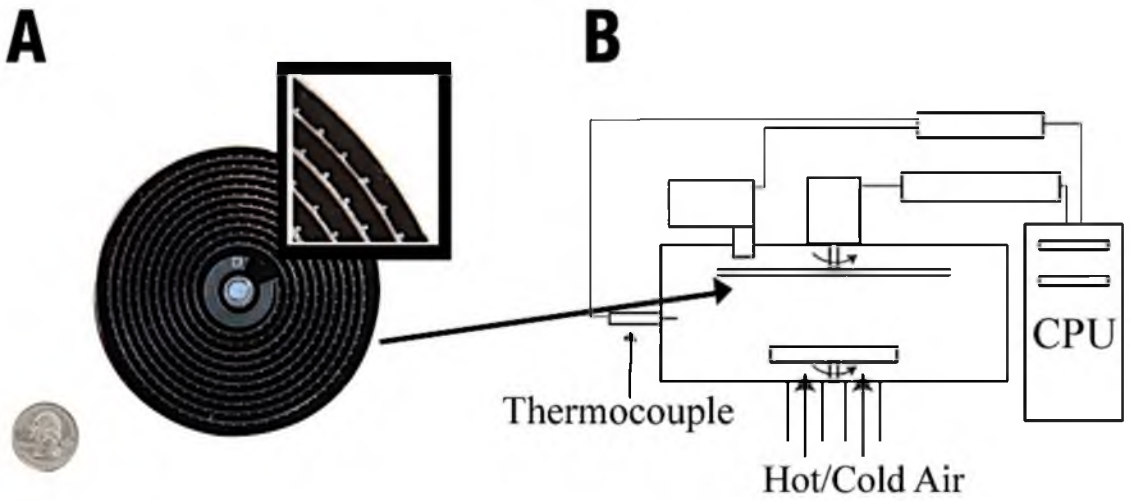

Figure 2.1: Experimental disk and thermocycler sketch. (A) One of the prototype disks. The wells were 500μm x 500μm x 125μm and the channels were 250μm wide. The DNA solution is loaded in the wide channel in the center of the disk and then distributed to all the wells by centrifugal force. (B) Side view schematic of spinning disk platform. Once the DNA solution is located in the wells, the PCR thermal cycling starts.

The disks had approximately 1000 individual square nanoliter-sized wells facing radially outward from a spiral channel. The disk was fabricated from three inexpensive plastic thin film sheets laminated together. A cutting plotter was used to pattern a layer of glycol-modified polyethylene terephthalate (PETG) and laminate that layer between two separate PETG layers. Some of their other prototypes included different materials, such as metalized mylar for the bottom layer, while maintaining plastic films for the top two layers. A schematic of the setup for the thermal cycling of the disk is shown in Figure 2.1.B. The disk, located on a small vertical shaft inside the thermocycler, was spun at 4000 rpm during loading in order to passively partition DNA template samples into the wells by centrifugation from the initial pipetted solution in the central reservoir. This process eliminates the need for valves and pumps. Once the disk was loaded, it was span at 2500 rpm during the remainder of the PCR thermal cycling process. The disk rotation promotes temperature uniformity and helps mitigate deformation due to high temperature gradients. Hot air from a fan is propelled into the chamber during the heating cycle. During the cooling process, jet impingement, using room-temperature air, cools the disk. Using this technology, Sundberg et al. achieved PCR cycle times of 33 sec [8]. However, a thorough thermal analysis of their prototype was not reported. The disk was spun to induce temperature uniformity and obtain higher heat transfer rates, yet the thermal processes were not optimized or justified. Another team [9] created a thermocycler for the same spinning disk setup that used radiation as the heat source and ambient

air convection for cooling. They were able to obtain higher heating rates (24 – 30 s/cycle), but once again, temperature uniformity and control were not reported.

Due to the significant advantages presented by the microfluidic spinning disk digital PCR platform, it is essential to develop a mathematical thermal model of the system to better understand the effects of the relevant parameters and that could be used to improve future designs. This paper presents just such a parameterization study. The effects of the radial location of the impinging air jet normal to the disk surface on the temperature uniformity of the disk and the heating/cooling time are presented. In a similar fashion, the effects of the air stream Reynolds number, which is a function of mass flow rate and the air jet outlet diameter are presented. Other parameters studied are the temperature of the impinging air jet, the spinning rate of the disk, and the volume of the PCR thermocycler.

2.3 Methods

Due to the complex physics governing the heat transfer in the spinning disk platform setup, it was necessary to resort to a computational numerical method. We used COMSOL Multiphysics, a commercial finite-element method (FEM) modeling software designed to solve transient heat transfer, among other physical phenomena, described by partial differential equations. Figure 2.2 describes a 2D representation of the modeled system.

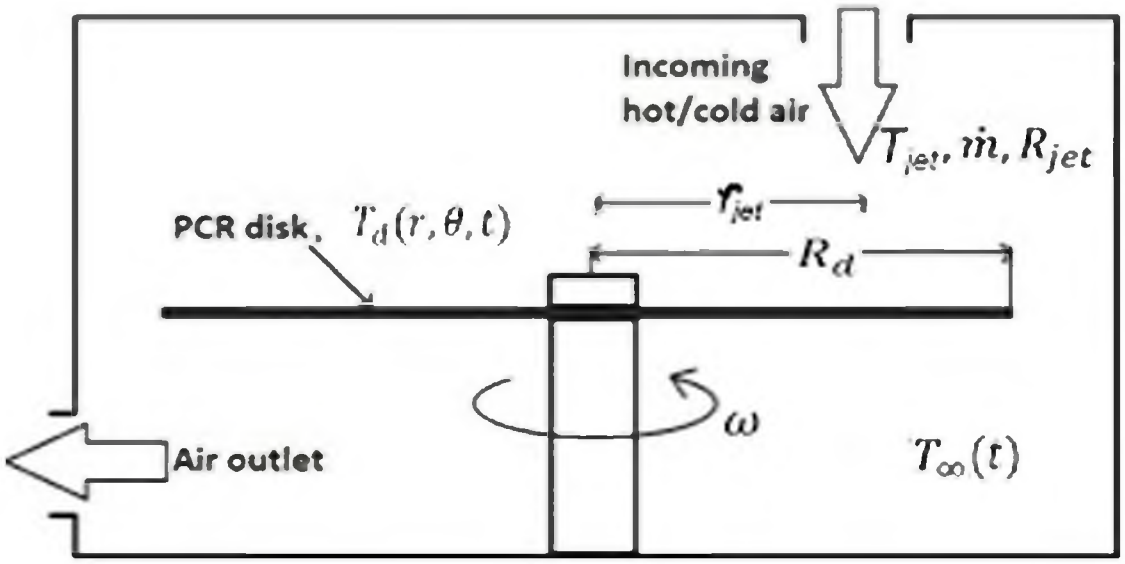

Figure 2.2: 2D schematic of COMSOL model. The air jet impinges normally on the disk at an off-center position. The disk spins at ω during the thermal cycling process. The air temperature change with time inside the thermocycler was also taken into account, $T_{box}(t)$.

2.3.1 Computational Model

2.3.1.1 Geometric Analysis

Computational numerical modeling (FEM included) requires a domain, or space, to be identified that identifies the area or volume, as well as the boundaries, on which the differential equations are to be solved. Within that domain, subdomains are created to represent different materials/substances in the system. The meshing framework, which identifies the locations for the desired solutions, is dependent upon the number and size of subdomains. As the mesh in a model becomes finer, required computer resources increase. If the temperature distribution and fluid motion in the nano-meter wells were desired, an extremely refined mesh would be required. Fortunately, the very small amount of DNA solution inside the individual wells remains relatively

stationary; thus, an analysis that incorporates micro-scale effects is not necessary.

Prior to creating a numerical model in COMSOL, analytical analyses revealed that temperature differences across the thickness of the disk (250 – 350 μm) are on the order of 0.1 °C. Moreover, heat transfer from the circumferential surface area of the disk, due to the extremely small area relative to the top and bottom surfaces, is negligibly low. These two findings greatly simplify the numerical model by allowing the thickness of the disk to be considered infinitely thin since radial heat conduction is much more significant than that in the vertical direction. Since the thermal diffusivity of the DNA solution (assumed to have thermal properties similar to water) is close to that for the plastic films, a single layer mesh (shell finite element formulation) is used to model the disk domain. A shell is a 2D mesh structure that functions in 3D space, giving the advantage of imposing boundary conditions on the mesh area rather than around its perimeter. As a result of this mesh simplification, computational time and cost are reduced by at least an order of magnitude compared to a mesh that represents the multilayer and helix-channel/wells geometry. Figure 2.3.A shows the mesh structure used for the analyses and results presented herein. Triangular mesh elements are used and the mesh is refined in regions of high temperature gradients, which correspond to the area immediately around the center of the heating/cooling air jet. The mesh elements do not vary dramatically throughout the remainder of the domain, however, due to the relative small area of the model.

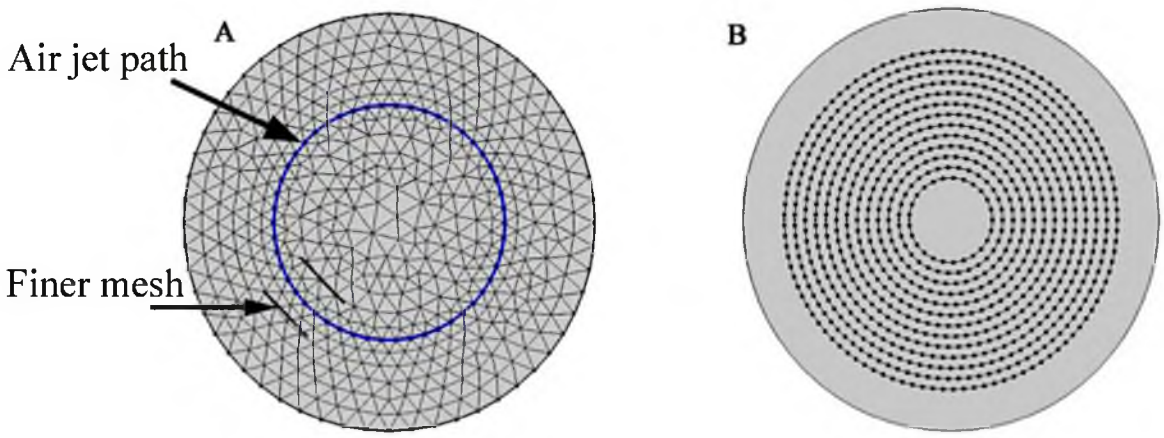

Figure 2.3: Mesh structure and data-retrieving model employed by COMSOL. (A) Mesh structure used to model disk. The bold circular line represents the midpoint of the trajectory that the heating/cooling air jet follows as the disk spins. Also, a finer mesh was designated near the air jet path due to high temperature gradients. (B) Computational representation of the disk where the black dots, which represent well locations, were the points where temperature data were extracted. The inner most circle of data points is at 20% of R_d and the outer most circle of data points is at 80% of R_d.

A mesh analysis was performed to determine an adequate triangular mesh size. Three different mesh sizes were considered: fine, regular and course, where the smallest element in the mesh grid was 0.0005 m, 0.0027 m and 0.0075 m, respectively. The course mesh yielded nearly equivalent results as fine mesh, with only negligible error. This is due to the presence of the second-order derivative of temperature as a function of radial distance in the conduction heat equation. When the temperature gradient has an exponential decay, it is approximated linearly within each triangular element (even in the course mesh) and therefore the results are the same.

Specific locations on the disk are selected to represent the location of the wells. These points are separated by 2 mm circumferentially in the computational model. Radially, they are spaced from 20 – 80 % of r_d. The

array of points where temperature data are extracted is shown in Figure 2.3.B.

2.3.1.2 Material Properties

Even though the shell model has no physical thickness, the computational model still requires material property values, namely density, ρ [kg m^{-3}], heat capacity, c_p [J K^{-1}], and thermal conductivity, k_d [W m^{-1} K^{-1}]. This dependence can be mathematically observed in eqn (1). The nominal model simulates a three-layer disk of a metalized mylar bottom layer and two upper layers of FR83-Black polycarbonate thin film sheets [2]. It was needful, therefore, to create a theoretical "hybrid" material with the appropriate mass and volume weighted averages of the properties of these two materials. Mylar properties were assumed to be equivalent to those for aluminum and the polycarbonate thin films were represented by PMMA properties. k_d was determined using a volume fraction weighting of the two thermal conductivities, but since both the metalized mylar and the polycarbonate layers have the same area, the property weighting is accomplished with a thickness fraction. The nominal thicknesses are 50 μm and 125 μm for the metalized mylar and each polycarbonate layer, respectively. These dimensions yield a 1/6 ratio for the mylar and polycarbonate thermal conductivities. Similarly, both ρ and c_p were determined using a mass fraction weighting of the two materials' properties. The final thermodynamic and transport hybrid properties are shown in Table 2.1.

Table 2.1 Individual properties and weighted average hybrid properties for the computational model.

Material Properties	Aluminum	PMMA	Hybrid
ρ [kg·m^{-3}]	2700	1190	1661
c_p [J·K^{-1}]	900	1420	1258
k_d [W·m^{-1}·K^{-1}]	201	0.19	33.7

2.3.1.3 Convective Boundary Conditions

Little insight can be gained from a steady state heat transfer simulation of the digital PCR disk since conditions to which it is exposed are constantly changing. Furthermore, since the heating/cooling air jet is off-center (not aligned with the axis of the disk), asymmetric thermal conditions always exist. Therefore, a transient heat transfer analysis for the disk is performed. The governing equation is the transient energy equation:

$$\rho d_s c_P \left(\partial T/\partial t\right) + \nabla_T(-d_s k_d \nabla_T T) = \dot{Q} \tag{1}$$

where d_s [m] is the thickness of the shell (the one-layer mono-material mesh is maintained), T [˚C] is the temperature as a function of time t [s] and location (r, θ) on the disk, and $\dot{Q}$ [W] is heat generation (which is zero in this case).

A constant convective boundary condition is imposed on both sides of the disk to account for the convection created by the rotating disk. The value of this convection coefficient, h_s, is dependent on the spinning rate of the disk, ω, by:

$$h_s = a k_a \sqrt{\omega/\nu} \tag{2}$$

Eqn (2) is valid for a laminar spinning Reynolds number [10] (transitional Reynolds number is strongly dependent on experimental conditions and ranges between $20x10^4$ and $32x10^4$), Re_s, defined as

$$Re_s = \omega r^2/\nu \tag{3}$$

The dimensionless constant *a* has a value of 0.33 and k_a and *v* are the thermal conductivity and the kinematic viscosity coefficients of air, respectively. Due to the negligible change of air properties between 50 and 100 ˚C, constant air properties at 80 ˚C are applied.

A second convective boundary condition was superimposed only on the surface that was exposed to the incoming perpendicular jet of cold or hot air. The impinging jet configuration is used in a wide variety of applications to achieve enhanced coefficients for convective heating and/or cooling [11]. An extensive review of available convection coefficient data for impinging gas jets has been perfomed [12, 13]. The spatial distribution of the surface heat transfer coefficient is generally characterized by a bell-shaped curve for which the Nusselt number, *Nu*, decays from a maximum value at the stagnation point or central axis of the air jet. *Nu* is related to the heat transfer coefficient, h_{jet}, as follows:

$$Nu = h_{jet}d_{jet}/k_a \tag{4}$$

Though most available data are provided in the form of empirical plots, some attempts have been made to fit as many data as possible into general

correlations [11]. However, the *Nu* radial decay is extremely dependent on the speed and mass flow rate of the jet, nozzle-to-surface distance and nozzle diameter. Considering the nominal impingement conditions of this study, a particular correlation [14] with similar experimental parameters valid for $5x10^3 < Re_{jet} < 60x10^3$ was employed. Data from [5] were curve-fit and eqn (4) was used to obtain the local h_{jet} distribution shown here:

$$h_{jet}(x,y,t) = A \cdot exp\left[-k_b\sqrt{(x+a_0)^2+(y+b_0)^2}\right] + c_0 \tag{5}$$

While the boundary layer induced by the spinning disk is constant at all times, the boundary layer induced by the impinging air jet maintains the same shape and magnitude but changes locations on the disk as the disk moves. Eqn (5) shows the dependence of h_{jet} on time. A, k_b and c_0 are curve-fitting constants, where a_0 and b_0 are defined as:

$$a_0 = R_{jet}\cos(\omega t) \tag{6}$$

$$b_0 = R_{jet}\sin(\omega t) \tag{7}$$

Eqns (6) and (7) reveal the time dependence and therefore eqn (5) is a bell-shaped curve that rotates symmetrically around the center of the disk at rate ω. The principle of relativity allows us to represent the spinning disk with a stationary impinging jet with a stationary disk and a moving air source. Eqns (2) and (5) are superimposed on the surface exposed to the air jet as the boundary conditions and eqn (2) alone is used for the opposite surface.

The driving potential for convection heat transfer on the top surface of

the disk is the temperature difference between the incoming air jet, T_{jet}, and the surface. The bottom of the disk is exposed to an ambient temperature, T_{∞}, which increases as a function of time as hot air fills the thermocycler. A transient energy analysis was performed for the thermocycler volume taking into account the air mass flow rate and box volume (given below). It was determined that T_{∞} approaches T_{jet} in approximately 3 – 6 sec, depending on the mass flow rate (i.e. Reynolds number of the incoming flow). This transient T_{∞} behavior and the resulting transient convection driving potential are included in the model, as an exponential decay equation, to more closely represent the physics of the PCR cycling process.

2.3.2 Time Step Analysis

A suitable time step for the analysis is dependent on the angular velocity of the disk. For example, if the time step were equivalent to the time for a single revolution, the simulation would be unable to capture the spinning physics of the actual model. Moreover, if the time step were smaller but not sufficiently small, the simulation would yield inaccurate results; however, extremely small time steps would unnecessarily increase computational memory and computational time. An error analysis, based on a 512 time-steps-per-revolution point of reference (i.e. error = 0), revealed that even 32 time steps per revolution would yield negligible error at minimal computational cost (see Appendix). The model therefore makes 32 time steps per revolution.

2.3.3 Model Validation

An analytical transient heat transfer analysis, based on the lumped capacitance method, was performed to validate the computational model for a cooling process. Applying the lumped capacitance assumption of a spatially uniform disk temperature $T(t)$, the first law of thermodynamics for the disk gives

$$-h_T A_s\left(T - T_{jet}\right) = \rho_d V c(dT/dt) \tag{8}$$

where h_T is the total combined convection coefficient due to spinning and the impinging air jet, A_s represents the exposed area of the disk, ρ_d, V and c are the density, volume and heat capacity of the disk, respectively, and t is time.

The solution to equation (8) can be obtained by rearranging the equation and integrating both sides from $t = 0$ to a final time, t_h (when the mean temperature of the disk reaches the annealing temperature). The solution is expressed as:

$$t = (\rho V c/h_T A_s) ln\left[\left(T_j - T_\infty\right)/(T - T_\infty)\right] \tag{9}$$

Equation (9) shows the relationship of t_h with three important variables: ω, T_∞ and Re_{jet}:

$$t_h \propto \omega^{-1/2} \tag{10a}$$

$$t_h \propto ln(T_\infty^{-1}) \tag{10b}$$

$$t_h \propto Re_{jet}^{-2/3} \tag{10c}$$

The same trends were obtained from the COMSOL model as will be shown in the next section.

2.4 Results and Discussion

Representative of typical conditions in PCR, the denaturing temperature is defined as 95 ˚C and the annealing temperature 55 ˚C. The extension temperature is defined to be 72 ˚C, but was not considered in the current study as a temporal parameter. Given the temperature range for a typical denaturing process, the desired uniformity criterion is defined as the condition when all "well" temperatures (locations defined in Fig. 2.3B) are 95 +/- 1 ˚C at t_h.

A nominal case is analyzed for comparison to the results from other studies with different parameters. Parameters for the nominal case are: air jet outlet radius (equal to the air jet radius), R_{jet} = 0.75 cm; radial location of air jet axis perpendicular to the disk, r_{jet} = 2.25 cm; PCR disk radius, R_d = 4 cm; air jet Reynolds number, $Re_{jet} = 10^4$; air jet mass flow rate, $\dot{m}$ = 0.002356 kg s^{-1}; PCR thermocycler box volume, V = 15.2 cm x 20.3 cm x 15.2 cm (6 in x 8 in x 6 in); disk spinning rate, ω = 2005 rpm; h_s = 31 W m^{-2} K^{-1}; and air jet temperature, T_{jet} = 100 ˚C, $T_\infty(t = 0)$ = 55 ˚C, T_{amb} = 25 ˚C. The nominal case yields a heating process time t_h = 8.56 s with all well temperatures meeting the uniformity criterion.

Figure 2.4 shows the temperature profiles on the disk at different times in the heating process. In all three images, the "X" represents the location of the center of the air jet as the disk rotates as a function of time. The

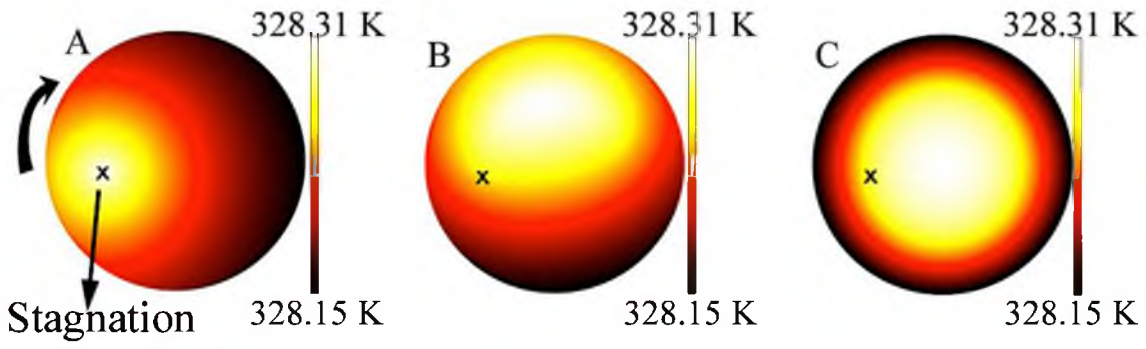

Figure 2.4: Thermal contour plot during the first revolution. The "X" represents the stagnation point of the air jet upon the disk as the disk spins clockwise. Each temperature legend bar is representative of the disk at that time. This revolution took ~0.03 sec. (A) shows the location of the concentration of heat resulting from the hot air jet impingement. This image was captured immediately after the hot air jet strikes the disk. (B) shows the temperature field after half a revolution. (C) shows the temperature field after one revolution and shows that the temperature field is almost axisymmetric. This phenomenon is in part due to the high disk angular velocity. The temperature field remains axisymmetric throughout the remainder of the heating cycle. Similar behaviour, but in the opposite direction, is observed for the cooling cycle.

temperature legend has different ranges for each of the three figures; however, the data indicate minimal temperature variation across the disk. This is expected since the first revolution for the nominal case takes less than 0.03 s and, therefore, limited heat transfer occurs.

Figure 2.4.A shows the temperature field on the disk at t = 9.37x10^{-4} sec, which is one time step immediately after the air jet first impinges on the disk. As expected, the hottest spot, represented by the lightest shade, is aligned with the axis of the air jet (arbitrarily initially located on the left side of the disk).

Figure 2.4.B shows the temperature field after half a revolution. It is interesting to note that the center of the air jet is not located at the epicenter of the temperature field. This "lag" is due to the heat capacitance of the disk

material as the disk is undergoing thermal storage of the initial heat input. This design parameter may be of interest to the microfluidic engineer if transient conditions are of importance.

Figure 2.4.C shows the temperature field after the first complete revolution. It indicates that the temperature distribution on the top surface of the disk is nearly axisymmetric. The temperature distribution at any time on the bottom of the disk is nearly equal to that on the top surface due to the infinitely thin assumption for the disk. After three or four revolutions, the temperature distribution becomes almost perfectly axisymmetric and remains that way throughout the rest of the heating process. Due to mathematical and physical symmetry of the heat transfer process, similar radially symmetric profiles, yet opposite in temperature, would be expressed for the cooling part of the cycle. By the end of a heating or cooling cycle, though the axial symmetry remains, the temperature difference across the disk is greater than at the start of the process, as will be shown later.

Since it is known that the disk temperature field is axisymmetric throughout most, and certainly by the end, of a heating or cooling ramp process, a simple 1D (radial) analysis will reveal strategic well and channel locations to obtain any desired uniformity criterion, even one more precise than +/- 1 ˚C at any desired end temperature. As opposed to a 2D or 3D analysis, 1D analyses are within the time and cost scope of many companies and/or research teams.

The effect on the heating process of different jet locations relative to the

disk center (r_{jet} = 0) is analyzed by varying r_{jet} from 0 to 3.25 cm. All other parameters for this analysis are the same as the nominal case. Figure 2.5 shows the effect r_{jet} has on the heating process time, t_h, and the maximum temperature difference across all wells, $\Delta T_{w,}$ which is representative of the well temperature uniformity. The time to complete one heating process increases nearly exponentially as the location of the heating air jet is moved away from the center of the disk. Defining the nominal case value as the datum, the percentage difference (as shown in eqn 11) is computed as:

$$\frac{t_h - t_{h,nominal}}{t_{h,nominal}} \times 100\% \qquad (11)$$

For the given range, 0 ≤ r_{jet} ≤ 3.25 cm, t_h decreases by 4.6% at its lowest value and increases by 5.6% at its highest.

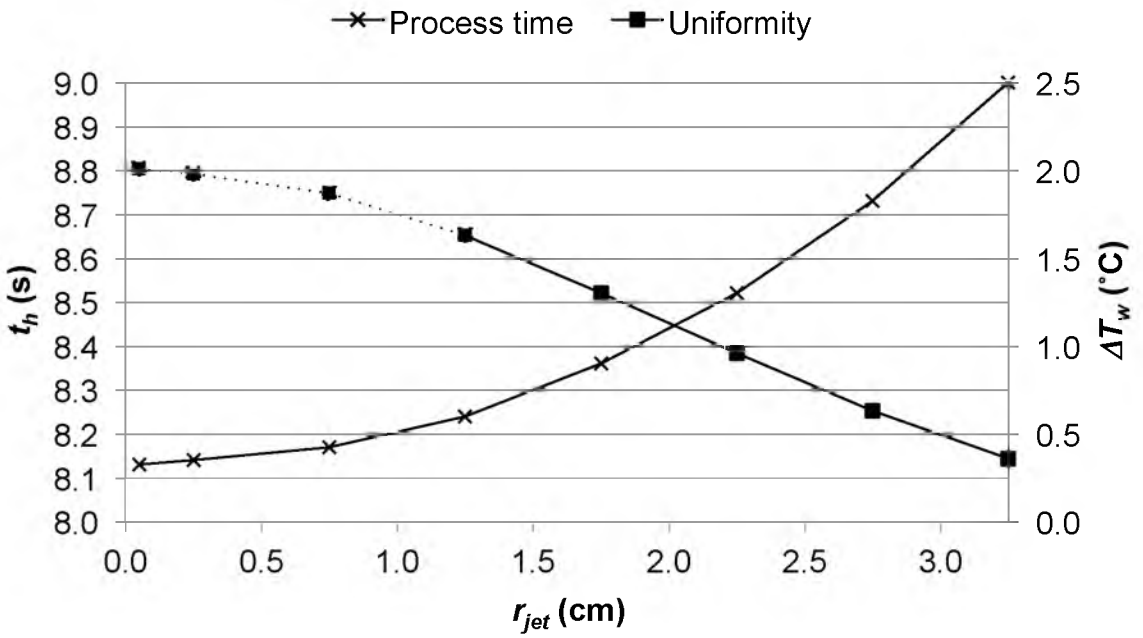

Figure 2.5: Effect of air jet location, r_{jet}, on heating process time and temperature uniformity.

This is an undesirable impact, however, since the greater t_h is, the longer the PCR process will take. On the other hand, increasing r_{jet} correlates with better temperature uniformity. For the given r_{jet} range, ΔT_w decreases by 63% from the nominal value at its lowest value and increases by 110%. This is a desirable outcome since small ΔT_w correlates with better temperature uniformity across the disk.

Furthermore, if the air jet is located 1.25 cm or closer from the disk center, ΔT_w falls outside 94 – 96 ˚C, which was defined as the temperature variation tolerance criterion. The dashed lines depict conditions in which the wells fall outside the uniformity criterion. As the air jet moves closer to the center, uniformity degrades. The approximate percentage of wells outside the ΔT_w tolerance at r_{jet} = 1.25 cm is 12% and at r_{jet} = 0 it is 17%. Clearly, there is a trade-off between heating process time and temperature uniformity. As shown by the percentage differences, r_{jet} affects ΔT_w much more than t_h, and the appropriate air jet location should be defined accordingly.

The effects of Re_{jet} on temperature uniformity and process time are shown in Fig. 2.6; all other parameters are taken as the values from the nominal case. The range of Re_{jet} is from $5\text{x}10^3$ to $60\text{x}10^3$. As Re_{jet} increases, t_h drops dramatically. A decrease in t_h with increasing Re_{jet} is naturally expected, but the data in Figure 2.6 show that the most significant t_h decreases occur in the $5\text{x}10^3$ – $15\text{x}10^3$ range, rather than near $60\text{x}10^3$. For the given range, $5\text{x}10^3 \leq Re_{jet} \leq 60\text{x}10^3$, t_h decreases by 57% and increases by 29% from the nominal value. For

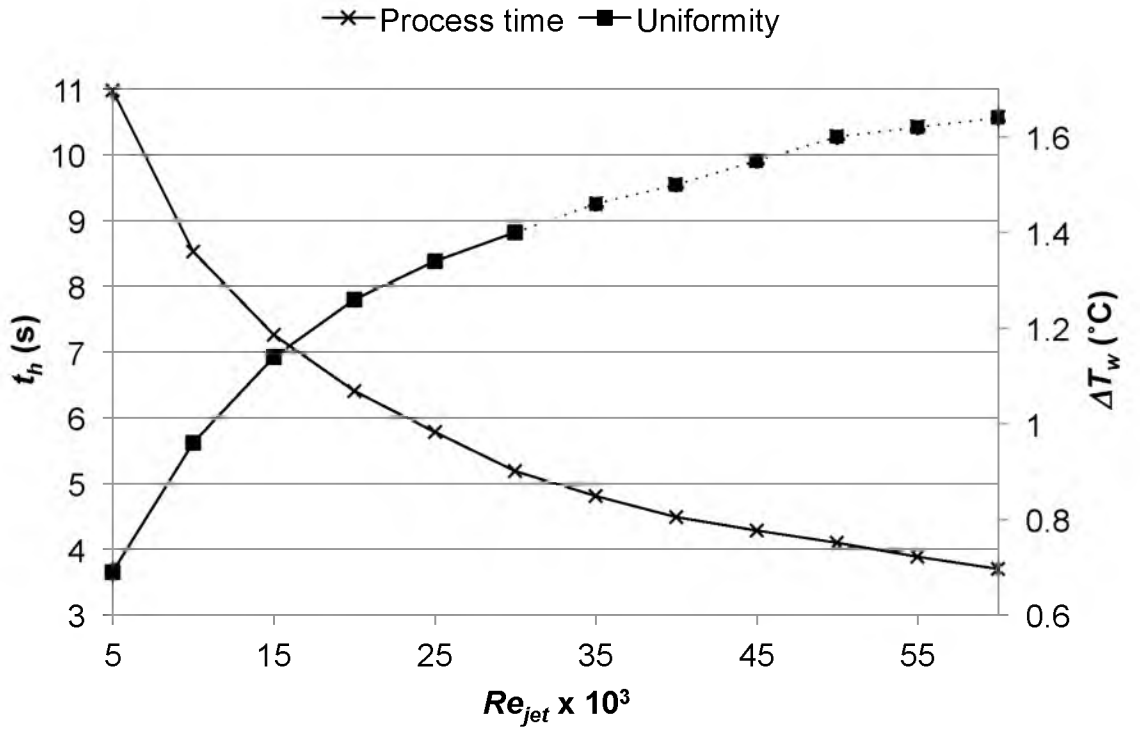

Figure 2.6: Effect of air jet Reynolds number, Re_{jet}, on the heating process time and temperature uniformity.

this dPCR configuration, uniformity is negatively affected by high values of Re_{jet} (> $35x10^3$). At Re_{jet} = $35x10^3$, 3% of the wells are outside the uniformity maximum tolerance criterion, while at Re_{jet} = $60x10^3$, 17% of the wells will theoretically not undergo the complete denaturing process, based on temperature alone. For the given Re_{jet} range, ΔT_w increases by 71% and decreases by 28% from the nominal value. As opposed to Figure 2.6, Re_{jet} affects both process rates and uniformity more equally. Furthermore, it is important to note that while Figure 2.6 shows poor temperature uniformity for Re_{jet} > $35x10^3$, this is only true for the nominal case at r_{jet} = 2.25 cm. As shown

in Figure 2.5, as r_{jet} increases, uniformity improves and therefore high Re_{jet} may still be considered if r_{jet} is increased accordingly.

Next, the impact of T_{jet} on the same heating process outcomes was analyzed with all other parameters equivalent to those in the nominal case. As shown in Figure 2.7, t_h decreases with an increase in T_{jet}, as validated by the analytical model. For the given range, 100 °C ≤ T_{jet} ≤ 135 ˚C, t_h decreases by 66%, while ΔT_w increases by 257%. Though t_h is greatly affected by the change, T_{jet} has more of an impact on ΔT_w. Surprisingly, for T_{jet} values as low as 105 ˚C, ΔT_w falls outside the tolerance criterion. This suggests that heating air jet temperatures should be maintained close to the desired denaturing temperature of the DNA solution, which unfortunately increases the PCR cycle time, but maintains the desired uniformity. However, depending on r_{jet}, T_{jet} may possibly exceed 105 ˚C while retaining the desired ΔT_w.

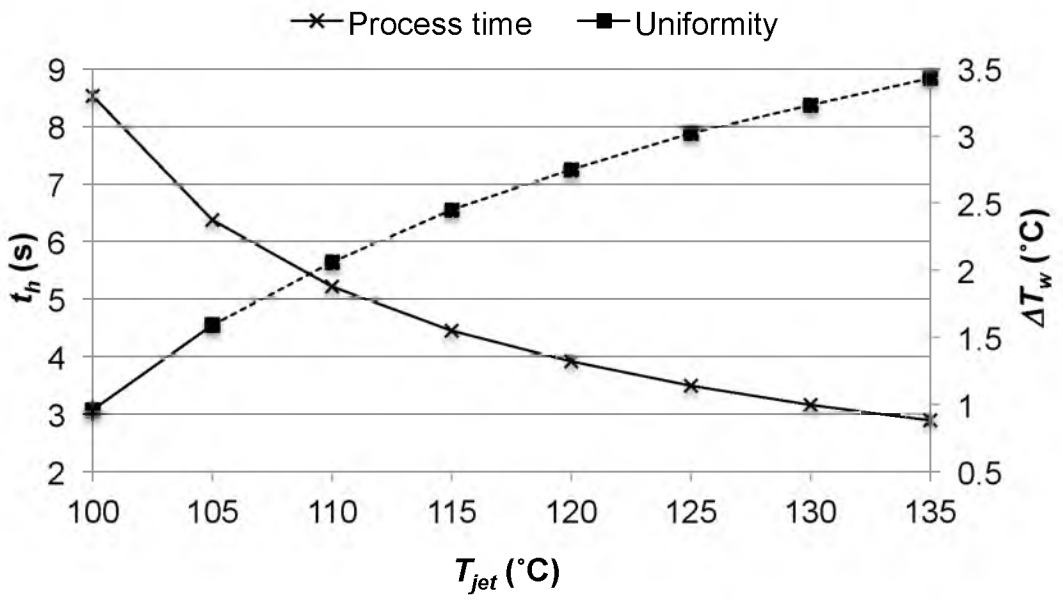

Figure 2.7: Effect of air jet temperature, T_{jet}, on heating process time and temperature uniformity.

As noted in eqn (2), disk angular velocity w affects the spinning heat transfer coefficient. Figure 2.8 shows the effects of ω on the system for all other parameters fixed at the nominal values. This is the only parameter that improves both the process time and temperature uniformity. None of the wells fall outside the temperature uniformity tolerance for the range of angular velocities explored. For the given range, $500 \leq \omega \leq 4000$ rpm, t_h decreases by 11% and increases by 20% from the nominal value, while ΔT_w decreases by 8.3% and increases by 9.4%. This important finding indicates that the disk can be rotated as fast as possible to increase heat transfer rates and temperature uniformity. However, microphysical or chemical parameters may also be affected by high ω, such as within the channels or wells, and should be considered before very high angular

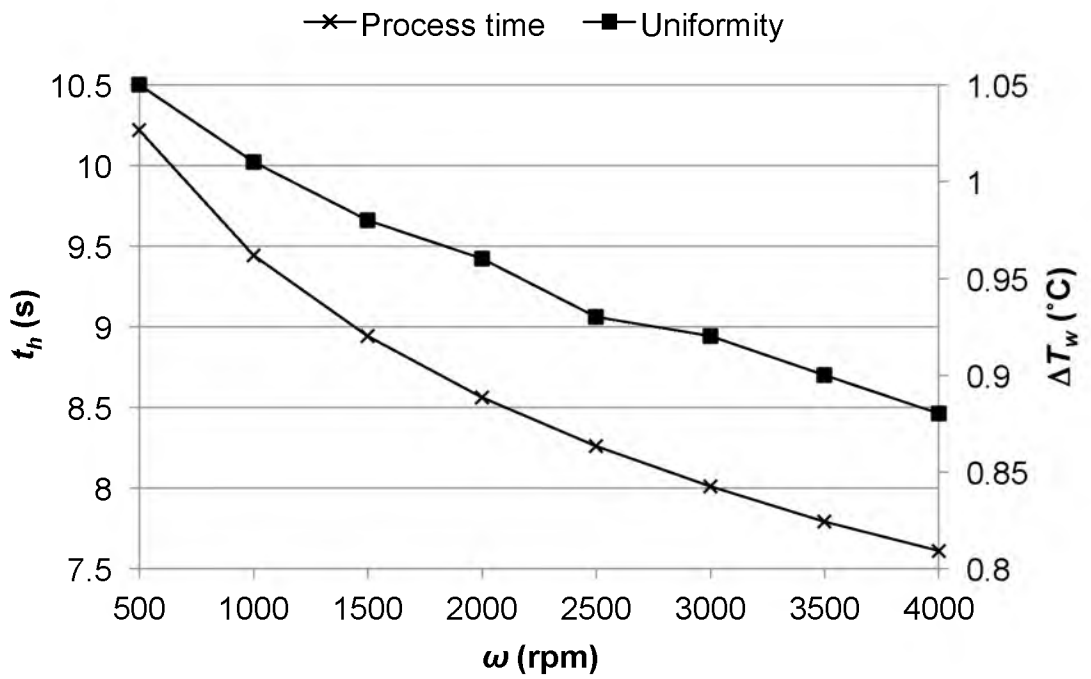

Figure 2.8: Effect of the disk angular velocity, ω, on the heating process time and temperature uniformity.

velocities are selected. Although both t_h and ΔT_w are positively affected by increasing ω, the improvement is not as significant as that obtained from other parameters, as highlighted above.

As noted previously, the thermocycler volume V impacts the transient response of the air temperature of the box, T_∞, which affects much of the convection heating/cooling of the disk (i.e., the surface opposite of the jet impingement). Volumes ranging from a decrease of 33% to an increase of 67% from our nominal value are considered. As expected, the more compact the PCR thermocycler, the smaller t_h becomes, but not significantly. Also, no significant changes to ΔT_w are observed for changes in V. These results indicate that one large PCR thermocycler could be designed to accommodate all disk sizes, since the thermocycler size does not have a detrimental effect on the smaller disk thermal cycle rates or temperature uniformity.

2.5 Conclusions

PCR is a biological process in which DNA segments are amplified exponentially. Digital PCR is a branch of such a process where only one DNA template is placed in given reaction volume, yielding greater precision over more conventional PCR methods. This study successfully completed the first computational thermal analysis of a spinning disk digital PCR technology. The effects of device design and operational parameters were analyzed, such as heating/cooling air jet location and temperature, air jet Reynolds number, disk angular velocity and thermocycler volume. A nominal case was created in

order to carry out a comparative study. Most of these parameters turned out to require trade-offs between thermal cycling rates and well temperature uniformity. That is, while the increase of certain parameters may improve cycle rates, they may degrade temperature uniformity across the disk, thereby producing undesirable results. Of particular design interest were the effects of the location of the heating/cooling air jet perpendicular to the disk, which up until this point had been unknown. The location does significantly impact the cycle times, but it also greatly affects temperature uniformity on the disk. The farther the jet is placed from the disk center, the more uniform well temperatures become after a heating/cooling process. It is recommended that these external parameters be advantageously controlled, with the others presented in this paper, to minimize cycling times and maximize the temperature uniformity of the thermal processes on the disk.

2.6 References

[1] T. Christopoulos, *Anal. Chem.*, 1999, **71**, 425R – 438R.

[2] S. Sundberg, Ph.D. Thesis, University of Utah, 2010.

[3] G. Pohl and I. Shih, *Expert Rev. Mol. Diagn.,* 2004, **4**, 41-47.

[4] E. Ottesen, J. Hong, S. Quake and J. Leadbetter, *Science*, 2006, **314**, 1464 – 1467.

[5] J. Qin, B. Fowler, W. Hwang, R. Jones and R. Ramakrishnan, Digital PCR on Fluidigm's New 200K Digital Array Chips, CA 2011.

[6] A. Huebner, S. Sharma, M. Srisa-Art, F. Hollfelder, J. Edel and A. deMello, *Lab Chip*, 2008, **8**, 1244 – 1254.

[7] J. Clausell-Tormos, D. Lieber, J. Baret, A. El-Harrak, O. Miller, L. Frenz, J. Blouwolff, K. Humphry, S. Koster, H. Duan, C. Holtze, D. Weitz, A. Griffiths and C. Merten, *Chem & Bio*, 2008, **15**, 427 – 437.

[8] S. Sundberg, C. Wittwer, C. Gao and B. Gale, *Anal. Chem.* 2010, **82**, 1546-1550.

[9] B. Gale, personal correspondence, University of Utah, 2008.

[10] T. Astarita and G. Cardone, *Int. J. Heat Mass Transfer,* 2008, **51**, 1562-1572.

[11] F. P. Incropera, D. P. Dewitt, T. L. Bergman and A. S. Lavine, in *Fundamentals of Heat and Mass Transfer*, John Wiley & Sons, 6th edn., 2007, ch 7, pp. 447-452.

[12] H. Martin, in *Adv. Heat Transfer*, ed. J. P. Hartnett and T. F. Irvine, New York, 1997, **13**.

[13] C. O. Popiel and L. Bogusiawski, in *Heat Transfer*, ed. C. L. Tien, V. P. Carey and J. K. Ferrell, New York, 1986, **3**.

[14] B. Hollworth and L. Gero, *J. Heat Transfer,* 1985, **107**, 910-915.

CHAPTER 3

CONCLUSIONS AND RECOMMENDATIONS

3.1 Summary

The field of MicroElectroMechanical Systems (MEMS) has proven to be a stepping-stone towards a vision shared by theoretical physicist Richard Feynman in 1959 when he asked, "What would happen if we could arrange the atoms one by one the way we want them?" [1]. Though not of biological nature at first glance, MEMS has contributed significantly to different aspects in the biological, chemical and medical sciences. One process in molecular biology that has found a niche with MEMS is the Polymerase Chain Reaction (PCR). The PCR process is a nucleic acid amplification technique in which templates of DNA or RNA are multiplied into the millions and billions from one single copy. This genetic manipulation has contributed to areas such as gene expression analysis, diagnosis of hereditary diseases, forensic science, detection of infectious disease and other areas. Digital PCR, a subbranch that has fine-tuned the advantages offered by conventional PCR, is a technology whose technological and scientific development will largely depend on MEMS advances. Digital PCR offers more precision, validity and efficiency than traditional PCR. The success of the PCR process is largely based on precise thermal control. The two thermal parameters studied in this project were temperature uniformity and process time. Several

results were discussed in how these two thermal parameters are affected by different variables such as disc rotational speed, air jet Reynolds number and PCR thermocycler volume. Other important studies were not included in Chapter 2, but are shown in the appendix, in form of figures and corresponding brief descriptions.

3.2 Conclusions

The computer model is set up where a hot air jet impinged perpendicularly on the disk at a distance from its center, r_{jet}, during the heating cycle. A similar setup was assumed during the cooling cycle with a cool air jet. r_{jet} was varied in the range from 0 to 3.25 cm. It was found that r_{jet} did not impact the heating cycle time greatly (~9% maximum change). However, temperature uniformity in the wells was affected dramatically (~173% maximum change). Due to the circular movement of the jet relative to the disk, heat concentrated towards the center of the disk. Therefore, smaller r_{jet} values yielded worse temperature uniformity. Uniformity is important because at high temperatures the DNA can be damaged and at low temperature the DNA double-strand may not completely separate. Therefore, equal well temperature (+/- 1 ˚C) is necessary for a successful PCR procedure.

The change in air jet Reynolds number impacted the heating process time and temperature uniformity approximately the same (approximately 90% maximum change for both) over the range of Re_{jet} considered ($5x10^3 – 60x10^3$). Higher Reynolds numbers induced faster cycle times, but reduced temperature uniformity. Well temperatures exceeded the desired +/- 1 ˚C band for Re_{jet} >

$35x10^3$. The behavior of the disk seemed to be extremely sensitive to the temperature of the incoming hot air jet. Surprisingly, at air jet temperatures of 105 ˚C or higher, many well temperatures exceeded the desired +/- 1 ˚C variation from the selected denaturing temperature. Also, changes to the air jet temperature affected temperature uniformity much more than cycle speed, with 257% and 66% changes, respectively. Lastly and uniquely, an increase in disk angular velocity improved both heating cycle time and temperature uniformity. Cycle time was twice as sensitive to angular velocity as temperature uniformity. PCR thermocycler volume was also analyzed, but did not yield significant changes to the process. This may indicate that specific PCR thermocycler volumes for individual disk sizes may not be necessary. The advantage this presents is that a single PCR thermocycler may accommodate several different disk sizes if necessary with minimal effect on thermal performance.

Due to the diversity offered by different heat transfer boundary conditions for this system, one ultimate optimized design and set of operational conditions cannot be provided. Different PCR processes may be designed for different performance outcomes, which would affect the choice of values used for the key parameters. However, this study presented the physical effects on the heating cycle time and temperature uniformity among the wells induced by five important parameters that can be controlled by the designer. It is important to consider these results when designing similar systems in order to better predict PCR thermal outcomes.

3.3 Future Recommendations

This project provides several insights into future designs in the microfluidic PCR area. However, as in all things, and certainly engineering projects, there are different ways in which this project could be further improved.

First, radiation heat transfer was not taken into account in the COMSOL model. It is known that at high convection heat transfer coefficients, radiation may be neglected. However, radiation was considered in earlier 1D models and proved to be significant at high temperature differences between the disk and the thermocycler temperature, even when convection was active. In this project, radiation was not taken into account due to the added complexity (computational time, programming efforts and memory space) it would add to convective boundary conditions alone, and was therefore considered beyond the scope of this study.

Another aspect that was neglected was the impact different disk materials could have on the cycle times and temperature uniformity. The few times materials were changed in the model, results showed significant variation in cycling time and temperature uniformity. These changes are due to the difference in thermodynamic and transport properties for the materials, such as thermal conductivity, density, and heat capacity. It is recommended that future materials tested fall within the general or "common" material realm for microfluidics, such as silicon-based polymers and certain metals.

The results presented in this study were validated through different analytical models. One of the most important models is the Lumped Capacitance

Method, a simple yet powerful 1D transient heat transfer analysis tool. However, both computational and analytical models are based on mathematical theory that at times differs from reality. This is due, among other things, to the limitations and assumptions created by the physical governing equations. It is recommended that an empirical validation of this model be performed to obtain insight into the limitations of the assumptions presented by both mathematical models.

In terms of boundary conditions, there is considerable potential work that can be done. First, the convective boundary condition due to spinning is only constant for laminar Reynolds numbers. The transitional Reynolds number, for the current system, typically occurs between $2x10^5$ and $3.2x10^5$. Only laminar spinning Reynolds numbers were considered in this study and it may be of interest to consider higher angular velocities that would result in turbulent flows. Also, only impinging jet Reynolds numbers below 60,000 were considered. This greatly simplified the current study since Reynolds numbers for impinging jets are very geometry dependent. In addition, Nusselt numbers for impinging jet convection are mostly empirical and Reynolds number dependent. However, it may be useful to consider higher impinging jet Reynolds numbers to increase the versatility of this model.

An interesting turbulent fluid phenomenon occurs at low nozzle-to-surface separations in which a second maximum *Nu* is formed radially along the boundary layer [2]. Because of the smaller relative drop in heat transfer convection coefficient, this may induce better temperature uniformity and

possibly significantly higher heat transfer rates. However, this case was not considered in the present study. This is further relevant and realistic, especially in microfluidic design, due to the continual search to dramatically reduce all dimensions.

Lastly, it is recommended that a future computational model closer represent Sundberg's thermocycler apparatus. As shown in Figure 2.1.B, a fan was placed immediately after the inlet to uniformly impact distribute the air on the disk. This effect was beyond the scope of the current project, but a computational model with this addition would give further insight into different or more effective ways of heating and cooling the disk.

3.4 References

[1] R. Feynman, "There's Plenty of Room at the Bottom", *Engineering and Science*, 1959.

[2] Incropera, F. P., Dewitt, D. P., Bergman, T. L., Lavine, A. S., 2007, "Fundamentals of Heat and Mass Transfer," 6th ed., Wiley, New York.

[3] S. O. Sundberg, C. T. Wittwer, C. Gao, B. K. Gale, *Anal. Chem.*, 2010, **82**, 1546 – 1550.

APPENDIX

Several analyses were conducted that were not included in the previous chapters. Selected results from these analyses are shown in this appendix. The phenomena reported include 1) the relationship between thermocycler ambient temperature and process times for heating, cooling and one complete cycle, 2) the effect of thermocycler volume on the heating and cooling process, 3) the time step analysis, 4) the temperature response for the first three complete cycles of the PCR process, and 5) the effect of different metals on heating process time. These analyses are deemed significant and further research and studies motivated by these results are encouraged.

Figure A.1 shows the effects of room temperature (T_{amb}) on the heating and cooling process times and cycle time (i.e., one complete cycle) when all other parameters have their nominal values. T_{amb} is also the initial temperature of the air inside the thermocycler, $T_{\infty}(t = 0)$, at the start of the PCR process. T_{amb} represents the air temperature outside the thermocycler and is assumed to be constant during thermocycler operation. In addition, T_{amb} represents the air jet temperature for cooling. Keep in mind that the air temperature inside the thermocycler will rise and fall as a function of time during the heating and cooling processes, respectively, but T_{amb} remains fixed. As T_{amb} increases, the heating and cooling process times decrease and increase, respectively. A more pronounced effect is manifested in the cooling cycle. At about T_{amb} = 50 °C, both

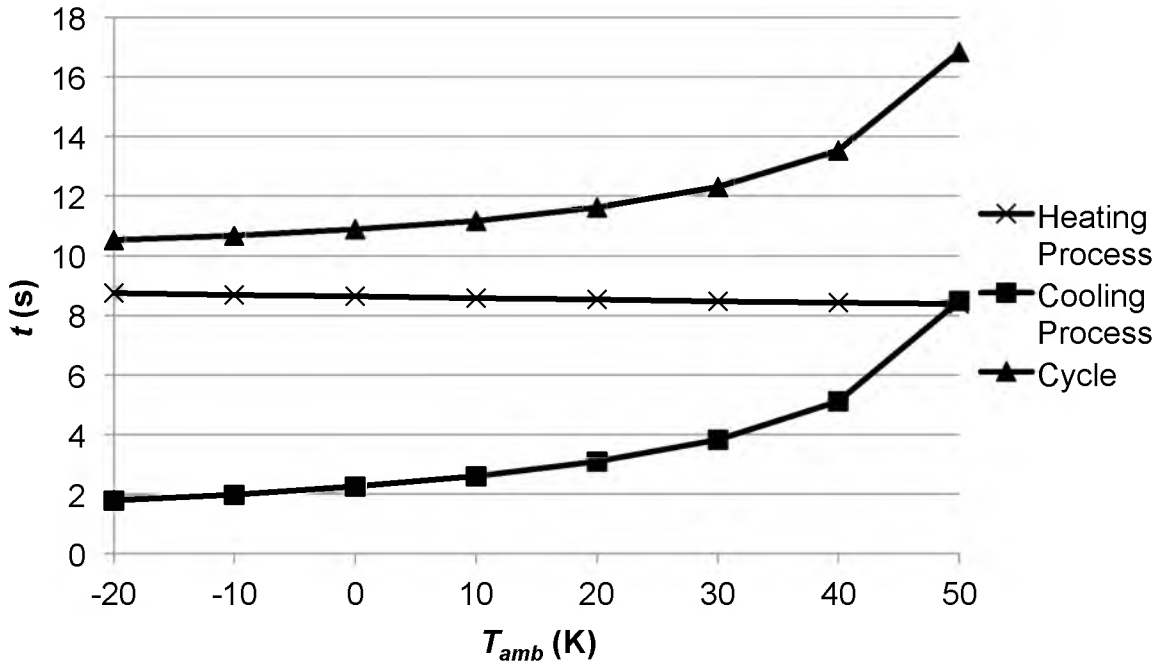

Figure A.1: Effect of ambient room temperature, T_{amb}, on heating and cooling process times. The heating process is maintained between 8 - 9 sec. The cooling process increases exponentially as the ambient room temperature increases from -20 to 50 °C. Cycle time is determined as a sum of heating and cooling process times.

processes are of equal time. This effect may be useful from a controls perspective. The overall cycle time (heating and cooling combined) does not show a significant increase between -20 and 20 °C, but it increases nearly exponentially for greater values of T_{amb}. Temperature uniformity in the wells remains within +/- 1 °C for all T_{amb}.

The effects of the PCR thermocycler volume V on heating and cooling process times are shown in Figure A.2. All parameters have nominal values for this analysis, with the exception of V. The dimensions [in^3] of the thermocycler are 6in x 8in x L_{box}in. As the volume increases, both heating and cooling process

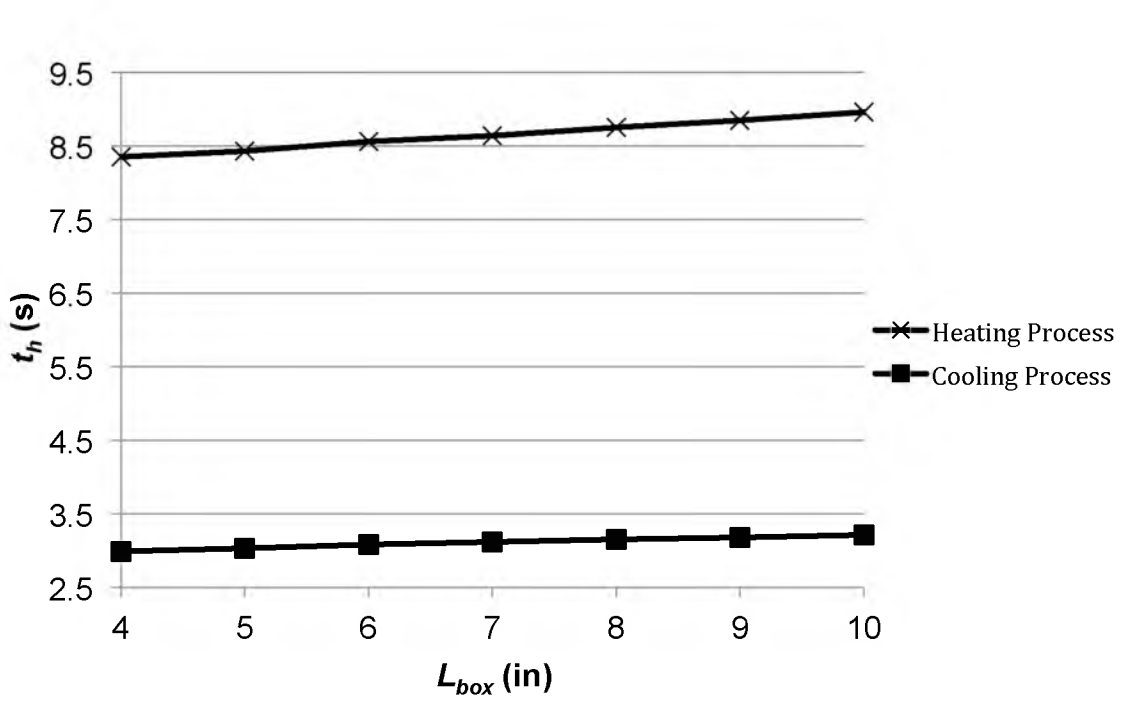

Figure A.2: Effect of thermocycler volume on heating and cooling process times. The process time is not changed dramatically as L_{box} increases by a factor of 2.5. Both the heating and cooling processes increase by approximately the same percentage.

times increase, as expected. With larger volume, the bulk ambient air temperature in the thermocycler responds more slowly to the energy input of the air jet. Both the heating and cooling process times increase monotonically with thermocycler volume; however, the changes are not very significant. This response suggests that a single size PCR thermocycler could be used for different disk sizes with no significant negative impact on effectiveness or overall process time.

Figure A.3 shows the time step analysis. The base case for the time step analysis was performed with 512 time steps per revolution; temperatures after one cycle serve as references for solutions with other time steps. The error

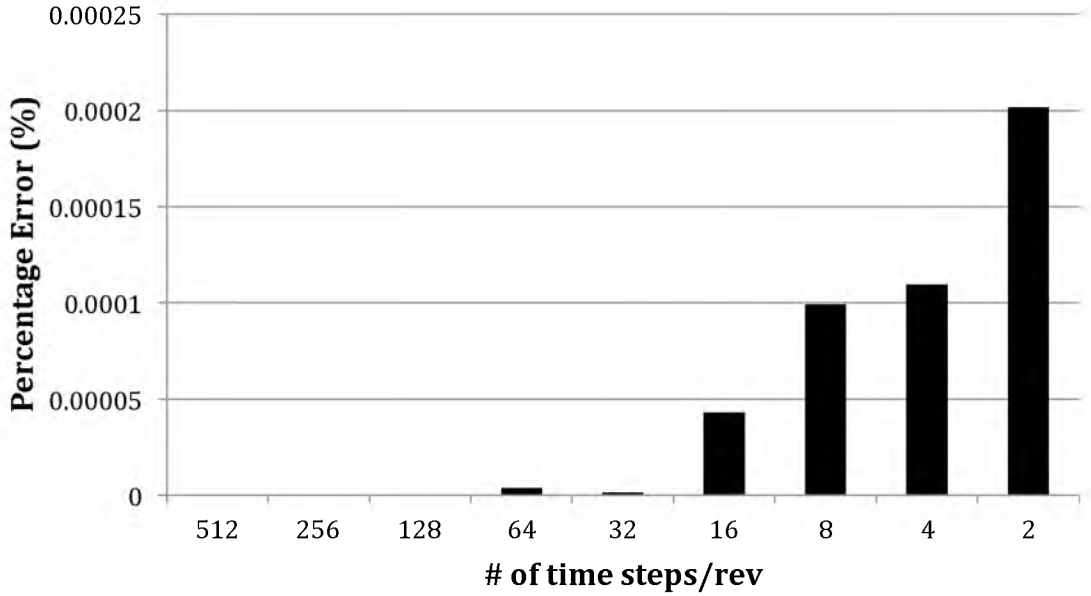

Figure A.3: Time step analysis. Thirty-two time-steps per revolution offered the least amount of error at inexpensive computational time and memory. The errors recorded in the vertical axis are values after one revolution. These errors are expected to increase as the revolutions increase in the computation. For instance, the total error induced after 1000 revolutions would be equal to the percentage error shown multiplied by 1000.

values shown are for one location after just one revolution. Error increases with the time step (the number of time steps per revolution decreases). At 16 time-steps/rev and smaller, significant error is induced. These errors propagate for each additional revolution and can potentially grow exponentially. Thirty-two time-steps/rev is used in this study since the temperature data show negligible error at reasonable computational time.

The temperature responses for the first three cycles of the nominal PCR case are shown in Figure A.4. Air temperature T_∞ is the temperature of the air inside the thermocycler, which changes as hot/cold air is injected into the thermocycler to heat/cool the disk. These transient temperature data show the

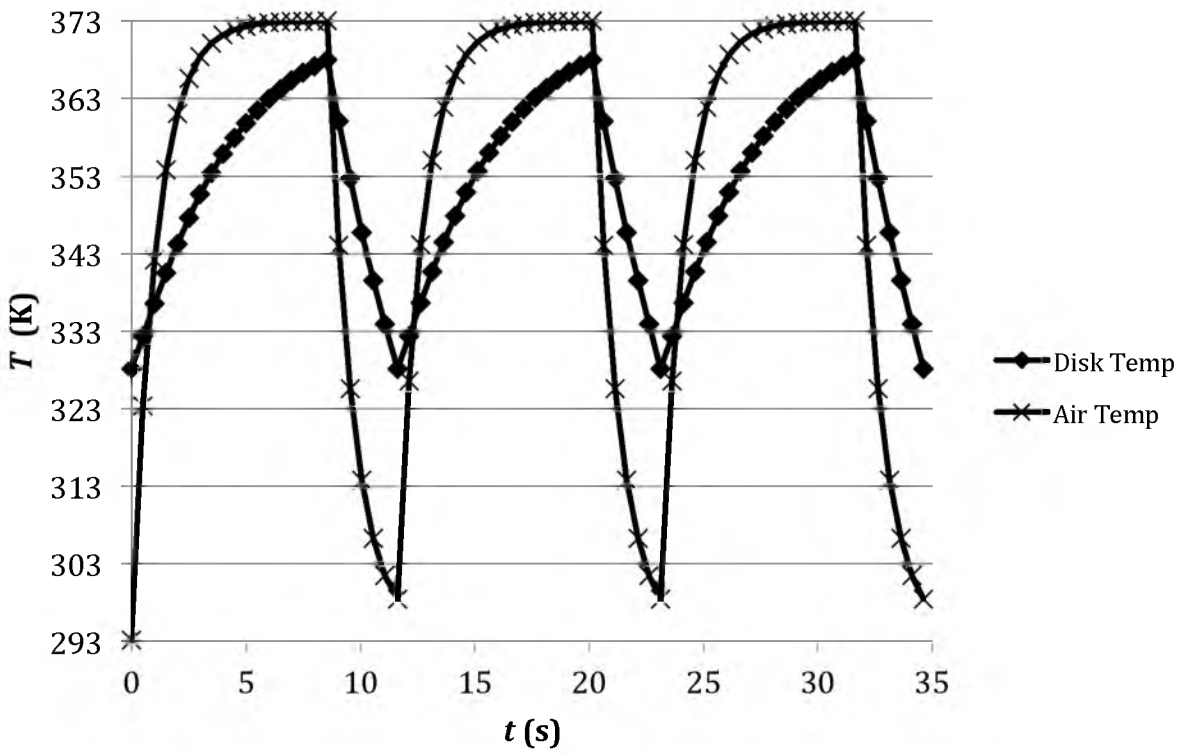

Figure A.4: First three cycles for the mylar/plastic hybrid disk. Disk Temp is the average disk temperature for all nodes, Air Temp is the air temperature T_∞ in the thermocycler. T_∞ = 20°C at the start of the process, T_{jet} = 100°C for heating, T_{jet} = 20°C for cooling, T_{avg} = 95°C for heating, and T_{avg} = 55°C for cooling.

relationship between the thermocycler air temperature and the average temperature of the disk as a function of time for the first three cycles. Though the air temperature inside the thermocycler is originally at room temperature (20°C), the system quickly reaches a steady state cycling condition following the first three cycles.

The effect of four different metallic materials (designed to be the bottom layer of the disk) on the heating process time is shown in Figure A.5. New hybrid properties were determined using volume and mass weighted averages of the metal and plastic materials, as described in Chapter 2. Layer thicknesses are the

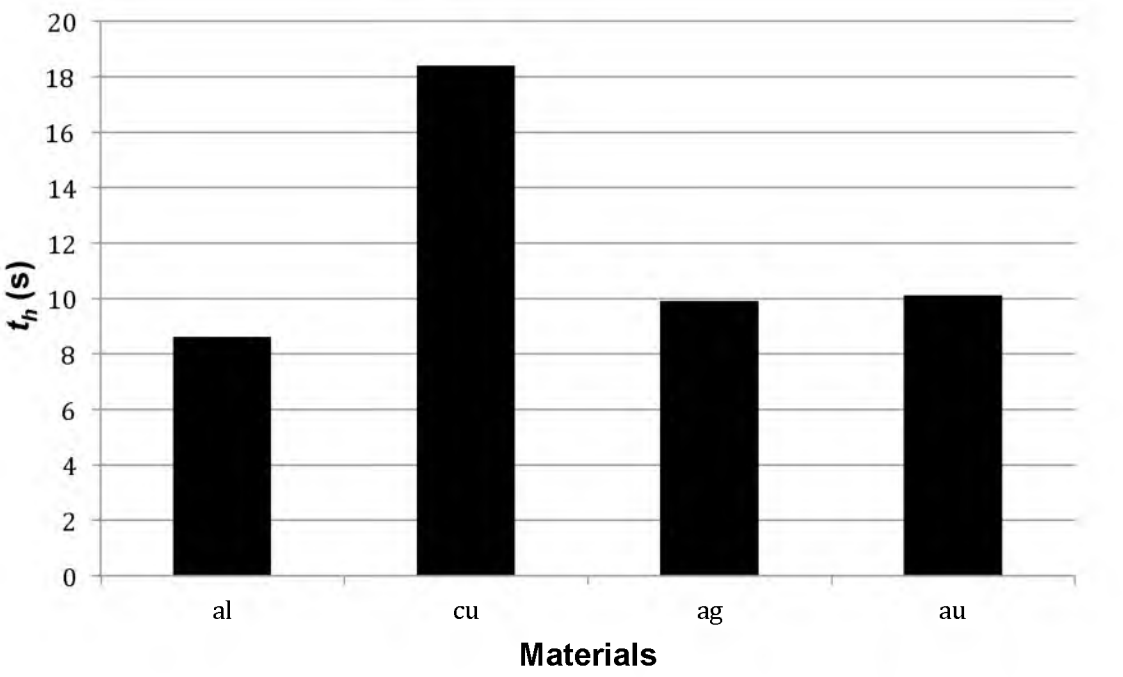

Figure A.5: Effect of material properties on process times. The different thermal diffusivity (material property) innate in each of these elements creates a different transient thermal response. Aluminum not only offers the fastest process time but also is the most cost-effective material.

same as in the nominal case (aluminum) as described in Chapter 2. Similarly, all other parameters are those associated with the nominal case. The heating process time for copper is over twice that for aluminum, which is nearly the same as that for the other two materials. All materials maintained the well temperatures within 95 +/- 1 °C at the end of each process. However, the uniformity (not shown) manifested a greater standard deviation (greater distribution) for aluminum than for any of the other metals. This may be attributed to the greater value of heat capacity, c_p, of aluminum compared to that of the other three metals. The data do not follow the expected trends based on the coefficient of the transient term, which is thermal diffusivity α, in the heat equation (eqn 1,

Chapter 2). Smaller values of thermal diffusivity (aluminum in this case) should produce the shortest heating process time, which is the case here. On the other hand, the slowest times are expected to be for the material with the largest thermal diffusivity. While copper produces the longest heating tine, it does not have the largest thermal diffusivity of the four materials. These unexpected results are likely due to the manner in which the physical domain was reduced to a shell consisting of a single substance with hybrid thermodynamic and transport properties. A more accurate assessment of the material effects could be investigated by considering a three-layer model that includes all material properties separately.